

Article

The Influence of $\text{SiO}_2 + \text{SiC} + \text{Al}(\text{H}_2\text{PO}_4)_3$ Coating on Mechanical and Dielectric Properties for $\text{SiC}_f/\text{MWCNTs}/\text{AlPO}_4$ Composites

Yan Zhu ^{1,2}, Feng Wan ^{1,2,*} , Jianhui Yan ^{1,2} and Hongmei Xu ^{1,2}

¹ School of Materials Science and Engineering, Hunan University of Science and Technology, Xiangtan 411201, China; 2020060428@mail.hnust.edu.cn (Y.Z.); jhyan@hnust.edu.cn (J.Y.); xhmhnust@163.com (H.X.)

² Hunan Provincial Key Laboratory of Advanced Materials for New Energy Storage and Conversion, Hunan University of Science and Technology, Xiangtan 411201, China

* Correspondence: wanfenghkd@163.com; Tel./Fax: +86-0731-5829-0732

Abstract: SiC fiber-reinforced AlPO_4 matrix ($\text{SiC}_f/\text{MWCNTs}/\text{AlPO}_4$) composites were fabricated using a hot laminating process with multi-walled carbon nanotubes (MWCNTs) as the absorber. A coating prepared from $\text{SiO}_2 + \text{SiC} + \text{Al}(\text{H}_2\text{PO}_4)_3$ was applied to the surface of the $\text{SiC}_f/\text{MWCNTs}/\text{AlPO}_4$ composites prior to an anti-oxidation test at 1273 K in air for 40 h. The anti-oxidation effect was verified by a three-point bending test, scanning electron microscopy, transmission electron microscopy, X-ray diffraction, and a dielectric property test. Anti-oxidation mechanism investigations revealed that the coating effectiveness could be attributed to three substances, i.e., SiO_2 , SiP_2O_7 , and $\text{SiO}_2 + \text{AlPO}_4$ solid solution from the reactions of $\text{SiC} + \text{O}_2 \rightarrow \text{SiO}_2 + \text{CO}$, $\text{SiO}_2 + \text{P}_2\text{O}_5 \rightarrow \text{SiP}_2\text{O}_7$ and $\text{SiO}_2 + \text{AlPO}_4 \rightarrow \text{solid solution}$, respectively.

Keywords: SiC fibers; oxidation; SiP_2O_7 ; solid solution



Citation: Zhu, Y.; Wan, F.; Yan, J.; Xu, H. The Influence of $\text{SiO}_2 + \text{SiC} + \text{Al}(\text{H}_2\text{PO}_4)_3$ Coating on Mechanical and Dielectric Properties for $\text{SiC}_f/\text{MWCNTs}/\text{AlPO}_4$ Composites. *Materials* **2022**, *15*, 5178. <https://doi.org/10.3390/ma15155178>

Academic Editors: Joseph Domblesky, Kai Jin and Zhenchao Qi

Received: 13 June 2022

Accepted: 22 July 2022

Published: 26 July 2022

Publisher's Note: MDPI stays neutral with regard to jurisdictional claims in published maps and institutional affiliations.



Copyright: © 2022 by the authors. Licensee MDPI, Basel, Switzerland. This article is an open access article distributed under the terms and conditions of the Creative Commons Attribution (CC BY) license (<https://creativecommons.org/licenses/by/4.0/>).

1. Introduction

Electromagnetic wave-absorbing materials, designed to decrease reflected electromagnetic radiation by absorbing electromagnetic waves and transforming it into other energy, is a topic of extensive interest in the aerospace and military fields [1–6]. Currently, the research for applications in high-temperature environments is the main topic for electromagnetic wave absorbing materials.

Continuous fiber-reinforced ceramic matrix composites (SiC_f/SiC [7], SiC_f/C [8], C_f/C [9], C_f/SiC [10], and $\text{SiC}_f/\text{AlPO}_4$ [11]), showing excellent fracture toughness, good thermal stability, and environmental durability, have been evaluated and modified for use as structural electromagnetic wave-absorbing materials. Especially, continuous SiC fiber-reinforced AlPO_4 ($\text{SiC}_f/\text{AlPO}_4$) composites have demonstrated good potential [12–14]. Their low dielectric constants provide the opportunity to tailor the dielectric properties and wave absorbing abilities by the addition of conductive fillers (carbon black, carbon nanotube, and graphene). However, the conductive fillers, SiC fibers, and C fibers are easily oxidized in oxidation environments, which limits the high-temperature application for ceramic matrix composites. Therefore, it is very important to form high-temperature antioxidant coatings on the surfaces of ceramic matrix composites to improve their oxidation resistance.

Currently, many efforts have been made regarding antioxidant coatings [15–17]. SiC ceramic coatings are usually used as bonding layers in environmental barrier coating (EBC) for C/SiC composite coatings owing to their good chemical and physical compatibilities with C/SiC composites [18,19]. However, micro-cracks develop owing to the difference in the thermal expansion coefficient between the SiC coating and C/SiC composites during the long oxidation process. To avoid the above problems, top coatings should be prepared

on the surface of the SiC coating to heal the micro-cracks, such as mullite, MoSi_2 , ZrSiO_4 , Y_2SiO_5 , CrSi_2 , and $c\text{-AlPO}_4$ top coatings. AlPO_4 ceramic, with many excellent properties such as a high melting point (above 1773 K), strong self-healing ability, low Young's modulus, and low oxygen permeability is usually an ideal high-temperature anti-oxidation coating material for many ceramic composites [20,21]. With the lowest low oxygen permeability in various oxide ceramics, SiO_2 ceramic also shows its advantage in the field of anti-oxidation coating [22,23].

Based on these results, a multi-composition coating, including SiC, SiO_2 , and AlPO_4 was prepared on the surface of $\text{SiC}_f/\text{MWCNTs}/\text{AlPO}_4$ composites in this paper. The anti-oxidation efficiency of the coating was proved and examined in detail.

2. Experimental Details

2.1. Materials

The SiC fiber was provided by the National University of Defense Technology (Changsha, China). The 2D SiC fiber cloths with a 40% fiber volume fraction were fabricated by Nanjing Glass Fiber Institute (Nanjing, China). MWCNTs used as conductive filler were supplied by the Shenzhen Nanotech port Co. Ltd., Shenzhen, China. The diameter of MWCNTs ranged from 20 to 80 nm, and length was 5–15 μm , and the purity was 95%. Figure 1a,b show the SEM image of 50 vol.% 2D SiC cloths and the TEM image of MWCNTs, respectively. The diameters of SiO_2 , Al_2O_3 , and $\beta\text{-SiC}$ powders are in the range of 1–5 μm .

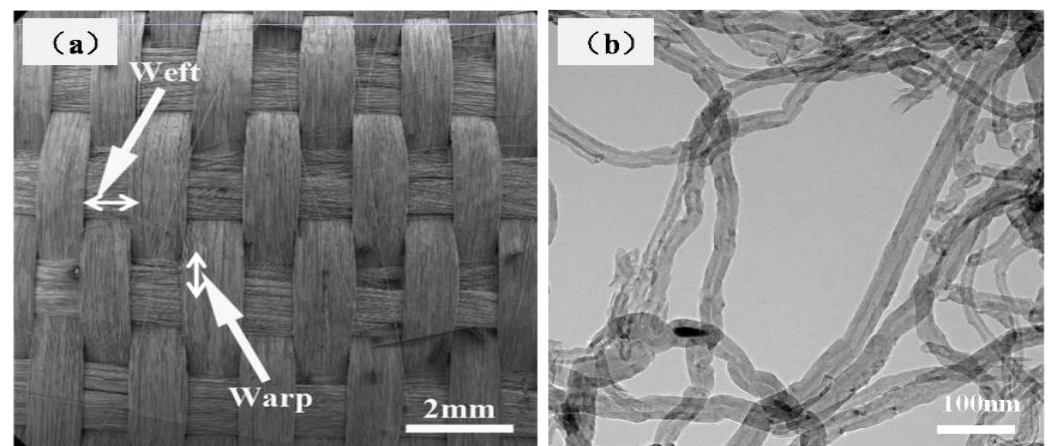


Figure 1. (a) 2D SiC fibers cloth and (b) TEM image of MWCNTs.

2.2. Preparation of the Composites

The $\text{Al}(\text{H}_2\text{PO}_4)_3$ solution, which is a precursor of AlPO_4 , was synthesized from aluminum hydroxide ($\text{Al}(\text{OH})_3$) and orthophosphoric acid (H_3PO_4 , 85%). $\text{Al}(\text{OH})_3$ at 1 mol was dispersed in deionized water, and H_3PO_4 (85%) at 3 mol was added into the suspension liquid to maintain the theoretical Al/P atomic ratio of 1:3. The mixed solution was then allowed to react at 90 $^\circ\text{C}$ for several hours, and the viscous $\text{Al}(\text{H}_2\text{PO}_4)_3$ solution was obtained. The MWCNTs and Al_2O_3 powders were uniformly mixed with as-received $\text{Al}(\text{H}_2\text{PO}_4)_3$ solution by ball milling for 4 h to obtain the slurry. The SiC fiber cloths were impregnated in the slurry. After air drying for 24 h, the 10 sheets of cloths obtained were laminated and hot pressed in a steel die at 100 and 200 $^\circ\text{C}$ for 1 h in turn. A pressure of 3 MPa was applied when the temperature reached 100 $^\circ\text{C}$, and such pressure was maintained until the end of hot pressing. Then, these samples were heated at a rate of 5 $^\circ\text{C}/\text{min}$ in a vacuum furnace to 500 $^\circ\text{C}$ for 1 h, and $\text{SiC}_f/\text{MWCNTs}/\text{AlPO}_4$ composites were obtained.

2.3. Preparation of the Coating

$\text{Al}(\text{H}_2\text{PO}_4)_3$ solution was mixed with the SiO_2 and SiC powders in the ratio 5:3:2 (w/w) $\text{Al}(\text{H}_2\text{PO}_4)_3:\text{SiO}_2:\text{SiC}$. After ball milling for 3 h, the obtained mixture was brushed onto the surface of $\text{SiC}_f/\text{AlPO}_4$ composites and dried at 373 K for 1 h prior to annealing at 1473 K

for 3 h at a heating rate of 283 K/min in vacuum atmosphere. After cooling at ambient temperature, the sample was given two infiltration–drying–annealing cycles to yield the coated $\text{SiC}_f/\text{AlPO}_4$ composites. Uncoated and coated $\text{SiC}_f/\text{AlPO}_4$ composites were heated to 1273 K in a muffle furnace. Treated samples were cooled to room temperature under ambient conditions.

2.4. Test Equipment

Morphology and microstructure were characterized by SEM (ZEISS Supra 55, Mainz, Germany) and TEM (G-20, FEI-Tecnai, Hillsboro, OR, USA). Phase evolution characterizations were determined by X-ray diffraction (XRD; X'Pert Pro, Philips, Amsterdam, The Netherlands).

The flexural strength of composites at room temperature was obtained by the three-point bending test, with a crosshead rate of 0.5 mm/min and an outer support span of 30 mm. The test was conducted following the general guidelines of ASTM standard C1341.

The complex permittivity values for the composites were measured based on the measurements of the reflection and transmission module between 8.2 and 12.4 GHz. The method was performed in the fundamental wave-guide mode TE₁₀ using rectangular samples (10.16 mm × 22.86 mm × 3.00 mm). After calibration using an intermediate of a short circuit and blank holder, the reflection and transmission coefficients were obtained using an automated measuring system (E8362B network analyzer). For dielectric materials ($\mu_0 = 1$, $\mu'' = 0$), the relative error varied between 1% (pure dielectric) and 10% (highly conductive material). The schematic diagram is shown in Figure 2.

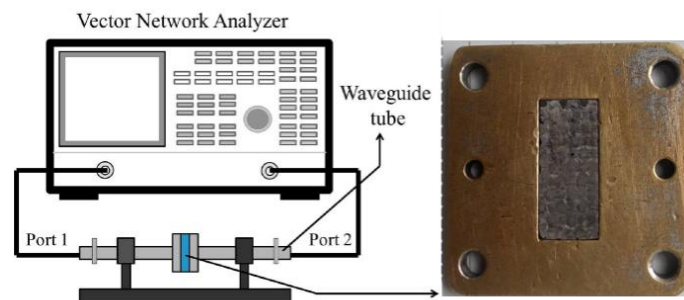


Figure 2. Schematic diagram for the dielectric property measurement.

3. Results and Discussion

3.1. Investigation of Bending Strength

The bending strengths for $\text{SiC}_f/\text{MWCNTs}/\text{AlPO}_4$ composites obtained by the three-point bending test are reflected in Figure 3.

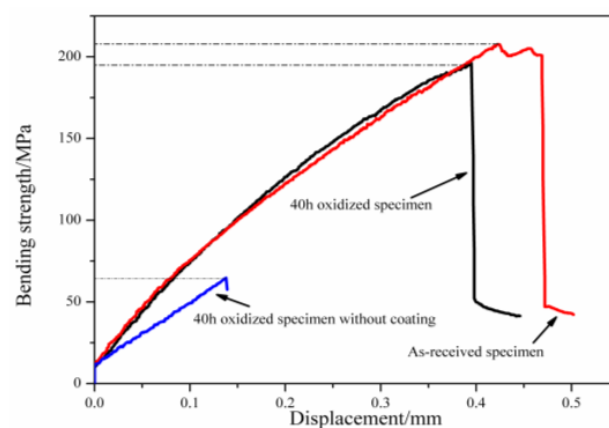


Figure 3. Typical stress–displacement curves of $\text{SiC}_f/\text{MWCNTs}/\text{AlPO}_4$ composites.

The three specimens initially showed an elastic response with increasing displacement. After reaching the maximum strength, the bending strength of the as-received specimen displayed an inelastic decrease before reducing abruptly. This differed from the curves of the oxidized specimens (with and without the coating), which showed a direct reduction in bending strength at maximum strength. The brittle fracture for the three curves could be attributed to the absence of an interface, which led to the loss of toughening mechanisms including fiber pull-out and debonding, and crack deflection. After oxidizing for 40 h, the bending strength of the coated specimen decreased from 205 to 190 MPa, and the displacement was reduced to 0.38 mm. These effects were due to the influence of high temperature on the SiC fibers. The specimen without the coating attained a bending strength of 60 MPa and displacement of 0.14 mm.

The corresponding fracture surface morphologies of the specimens (with and without the coating) subjected to oxidizing conditions are given in Figure 4. The fracture surface of the coated specimen was smooth and little fiber pull-out was observed (Figure 4a). The cross sections of SiC fibers were complete and clearly visible. Figure 4b,c show the SEM and TEM pictures of uncoated SiC_f/MWCNTs/AlPO₄ composites undergoing 40 h oxidation. Obviously, a strong bond occurred and a reaction zone was formed between the AlPO₄ matrix and SiC fiber, which could be attributed to the reaction of the AlPO₄ matrix and SiO₂, produced from the oxidation of SiC.

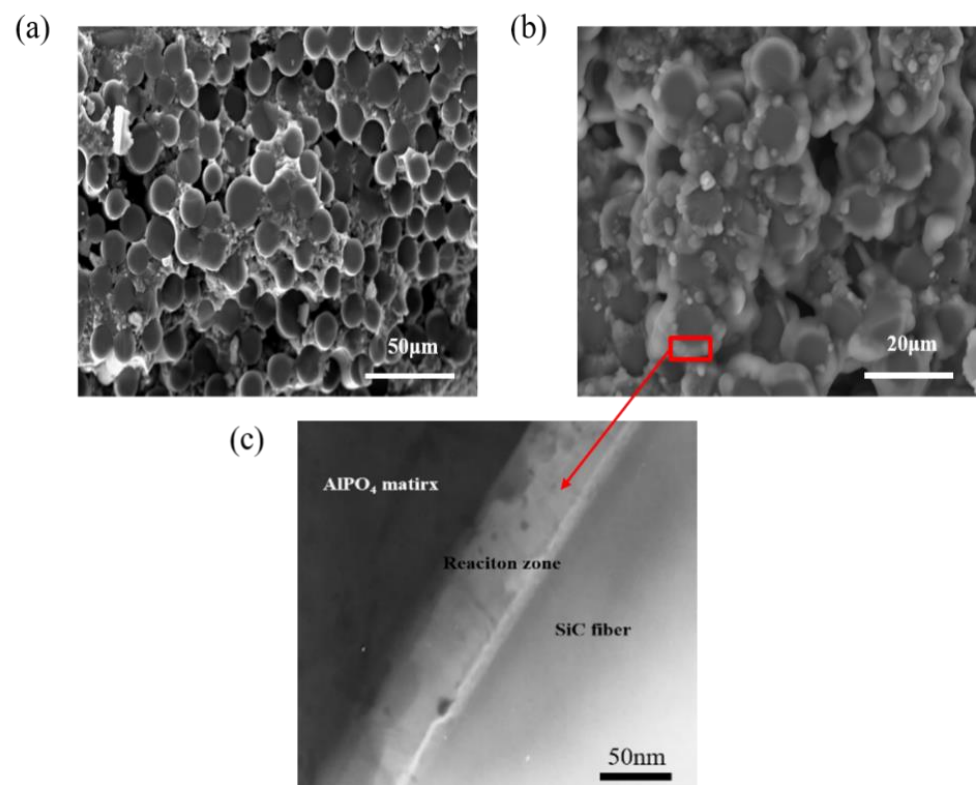


Figure 4. (a) SEM image of coated SiC_f/MWCNTs/AlPO₄ composites after oxidization, (b) SEM images of uncoated SiC_f/MWCNTs/AlPO₄ composites after oxidization, (c) TEM images of uncoated SiC_f/MWCNTs/AlPO₄ composites after oxidization.

3.2. Investigation of Dielectric Property

The real part (ϵ') and imaginary part (ϵ'') of the complex permittivity for the coated SiC_f/AlPO₄ composites are shown in Figure 5. Notably, Sample 1 denotes the coated SiC_f/AlPO₄ composites without MWCNTs added. Sample 2 denotes the coated SiC_f/AlPO₄ composites with 1.5 wt.% MWCNTs added. Sample 3 denotes the coated SiC_f/AlPO₄ composites with 1.5 wt.% MWCNTs added, which undergo 40 h oxidization.

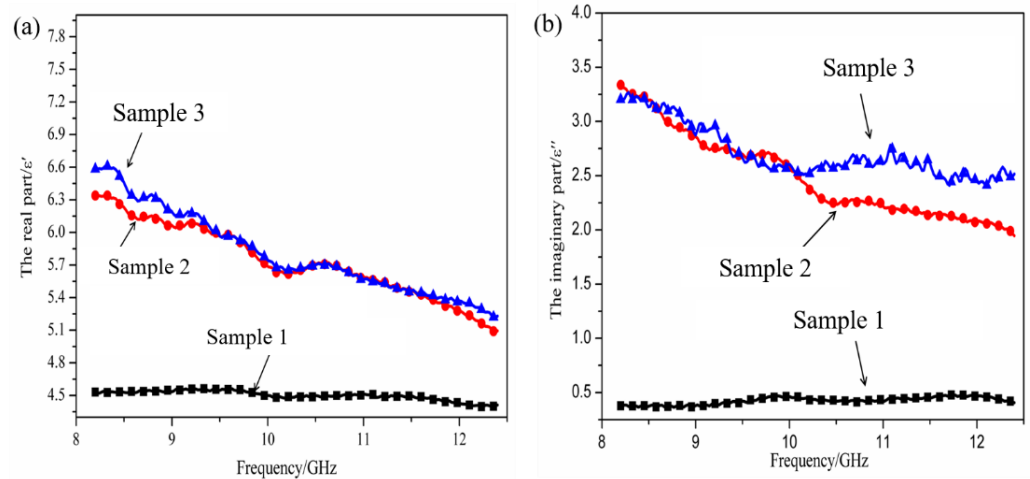


Figure 5. The complex permittivity values for the coated $\text{SiC}_f/\text{MWCNTs}/\text{AlPO}_4$ composites: (a) the real part (ϵ'), (b) the imaginary part (ϵ'').

The complex permittivity values of pure $\text{SiC}_f/\text{AlPO}_4$ composites (no coating and MWCNTs) have been discussed in [14]. The value of ϵ' was in the range of 3.6–4.1 and the value of ϵ'' was in the range of 0.1–0.2. The values of ϵ' and ϵ'' were small due to the insulated AlPO_4 matrix, which was observed in Table 1. After the introduction of the coating, the ϵ' and ϵ'' values for the $\text{SiC}_f/\text{AlPO}_4$ composites were in the range of 4.2–4.5 and 0.2–0.5 within the entire X-band, respectively. Compared to the result of Sample 1, the values of ϵ' and ϵ'' showed little change, which proved that the introduction of the coating had little influence on the dielectric property. This was ascribed to the low dielectric constants of the coating substances, reflected in Table 1. With the introduction of 1.5 wt.% MWCNTs, the ϵ' and ϵ'' for the coated $\text{SiC}_f/\text{MWCNTs}/\text{AlPO}_4$ composites ranges increased from 4.2–4.5 to 5.0–6.3 and 0.2–0.5 to 1.8–3.6, respectively. The main reasons can be given next.

Table 1. The dielectric constants of several substances.

Dielectric Constant	Substance			
	AlPO_4	$\text{SiO}_2\text{-AlPO}_4$ Solid Solution	SiP_2O_7	SiO_2
ϵ'	4.0–4.3	3.8–4.2	2.0–2.4	3.4–3.7
ϵ''	0.1–0.3	0.1–0.3	0.1–0.2	0.2–0.4

Complex permittivity is expressed by the following equation: $\epsilon = \epsilon' - j\epsilon''$. ϵ' is an expression of the polarization ability of a material. ϵ'' is an expression of the capacity of dielectric losses, which comprise polarization loss and electric conductance loss. The complex permittivity affects the absorbing wave property. When the value of ϵ' is too high, the electromagnetic wave cannot enter the composites, leading to a poor absorbing wave effect. When the value of ϵ'' is too small, the electromagnetic wave cannot be consumed, leading to a poor absorbing wave effect. So, a suit value of ϵ''/ϵ' is needed to satisfy the impedance matching rule.

According to the Debye theory of the dielectric, ϵ' and ϵ'' of the composites can be calculated as follows:

$$\epsilon' = \epsilon_\infty + \frac{\epsilon_s - \epsilon_\infty}{1 + \omega^2 \tau^2} \quad (1)$$

$$\epsilon'' = \frac{(\epsilon_s - \epsilon_\infty)\omega\tau(T)}{1 + \omega^2\tau(T)^2} + \frac{\sigma(T)}{\omega\epsilon_0} \quad (2)$$

where ϵ_s is the static permittivity, ϵ_∞ is the permittivity at the high-frequency limit, ω is the angular frequency, τ is the relaxation time, $\sigma(T)$ is the temperature-dependence electrical conductivity, and ϵ_0 is the dielectric constant in a vacuum.

As described in Formulas (1) and (2), ϵ' was determined by the relaxation time (τ). ϵ'' was determined by both the relaxation time (τ) and electrical conductivity of the composites ($\sigma(T)$). The possible polarization mechanisms at the microwave frequency included electronic, atomic, relaxation, and space charge polarizations. The contribution of atomic and electronic polarizations to permittivity was small and negligible. The effect of space charge polarization on the GHz range was lost because a long duration of time was required to establish polarization. So, the increase in ϵ' could be attributed to the electronic relaxation polarization enhanced by the MWCNTs. The introduction of MWCNTs not only brought the electronic relaxation polarization, but also made the electrical conductivity of the composites increase by free electrons shifting and hopping, which explains the increase in ϵ'' .

After 40 h oxidization, the values of ϵ' and ϵ'' for the coated $\text{SiC}_f/\text{AlPO}_4$ composites with 1.5 wt.% MWCNTs showed little change compared with the values before oxidation. These results showed that the MWCNTs were still present and functional. These findings demonstrated that the anti-oxidation effect of the coating was effective for the $\text{SiC}_f/\text{MWCNTs}/\text{AlPO}_4$ composites in an oxidizing environment at 1273 K.

3.3. Investigation of the Coating

Figure 6a shows the fracture surface image of coated $\text{SiC}_f/\text{MWCNTs}/\text{AlPO}_4$ composites before oxidization. The coating showed a strong bond with the AlPO_4 matrix, and no obvious boundary was distinguished (indicated by the black arrows). At the same time, fiber pull-out was observed in the image, which proved that SiC fibers had no reaction with the AlPO_4 matrix and the coating was effective. Figure 6b shows the surface image of the coating after preparation. It was observed from Figure 6b that the coating was dense and smooth, which showed a glassy state. No holes and cracks existed.

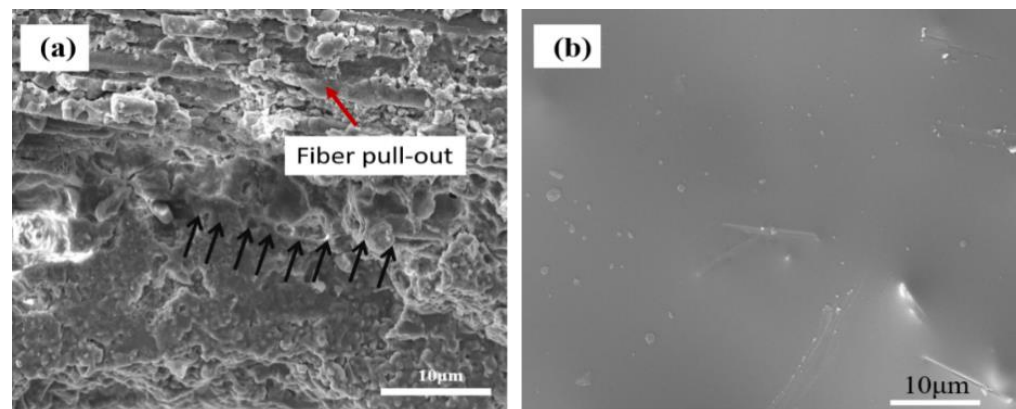


Figure 6. (a) The fracture surface image of coated $\text{SiC}_f/\text{MWCNTs}/\text{AlPO}_4$ composites and (b) the surface image of the coating before oxidization.

According to the phase diagram of $\text{AlPO}_4\text{-SiO}_2$ [23], some phases of solid solution (C- AlPO_4 solid solution, T- AlPO_4 solid solution, Cr- SiO_2 solid solution, and Tr- SiO_2 solid solution) might be formed when the preparation temperature of the coating was maintained at 1273 K, and these were dependent on the content of AlPO_4 and SiO_2 in the mixture. Consequently, this result was theoretically responsible for the strong bond between the AlPO_4 matrix and the coating.

The XRD spectrum of reaction products derived from the $\text{Al}(\text{H}_2\text{PO}_4)_3$ solution and SiO_2 is reflected in Figure 7. Four major peaks around 2θ values of 20.4° , 24.2° , 25.9° , and 30.4° (at 10 wt.% SiO_2) were homologous with the crystal phase of $\text{Al}(\text{PO}_3)_3$ and decreased in intensity with the increasing content of SiO_2 and were absent at 40 wt.% SiO_2 . However,

the intensity of the two peaks around 2θ values of 20.8° and 26.5° increased. Supposing these peaks were ensured to be SiO_2 , the disappearance of $\text{Al}(\text{PO}_3)_3$ peaks could not be accepted; if they are ensured to be AlPO_4 (i.e., decomposition products of $\text{Al}(\text{PO}_3)_3$), the disappearance of SiO_2 peaks could not be accepted. Hence, it was concluded that the SiO_2 reacted with AlPO_4 to form a solid solution, which was responsible for the diffraction peaks in the XRD spectrum of 40 wt.% SiO_2 . The continuous decomposition and final exhaustion for $\text{Al}(\text{PO}_3)_3$ was attributed to the consumption of AlPO_4 from an abundance of SiO_2 . Hence the results given in Figures 4b and 6b experimentally confirm that the SiO_2 - AlPO_4 solid solution was tightly correlated with the strong bond between the AlPO_4 matrix and the coating.

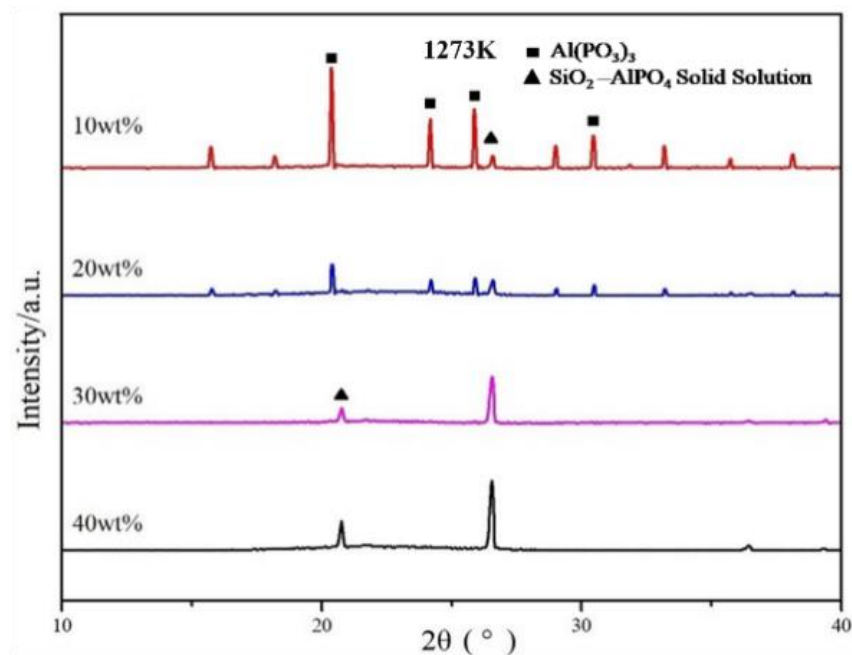


Figure 7. The XRD spectrum of reaction products derived from $\text{Al}(\text{H}_2\text{PO}_4)_3$ solution and SiO_2 .

The presence of low melting point SiP_2O_7 , derived from the reaction of SiO_2 and P_2O_5 ($\text{Al}(\text{PO}_3)_3 \rightarrow \text{AlPO}_4 + \text{P}_2\text{O}_5$), also strengthened the bonding within the coating and filled the holes and cracks in the coating to make it be a smooth, dense, and glassy state. This could be confirmed by the phase diagram of SiO_2 - P_2O_5 [14]. These two chemical reactions contributed to the formation of a dense coating.

Figure 8a shows the fracture surface image of coated $\text{SiC}_f/\text{MWCNTs}/\text{AlPO}_4$ composites after 40 h oxidization. The reaction of the AlPO_4 matrix and the SiO_2 filler strengthened the bond between the matrix and coating. Figure 8b shows the surface image of the coating after 40 h oxidization. It was observed from Figure 8 that the coating was still dense and smooth, which showed a glassier state. No holes and cracks existed due to the fill of low melting point SiP_2O_7 . On one hand, the routes of oxygen diffusion were filled due to the absence of holes and cracks; on the other hand, the efficiency of oxygen diffusion was decreased due to the SiO_2 , which was composed of the raw materials SiO_2 and reaction SiO_2 from the oxidization of SiC . These results proved that the coating was effective in preventing composite oxidization.

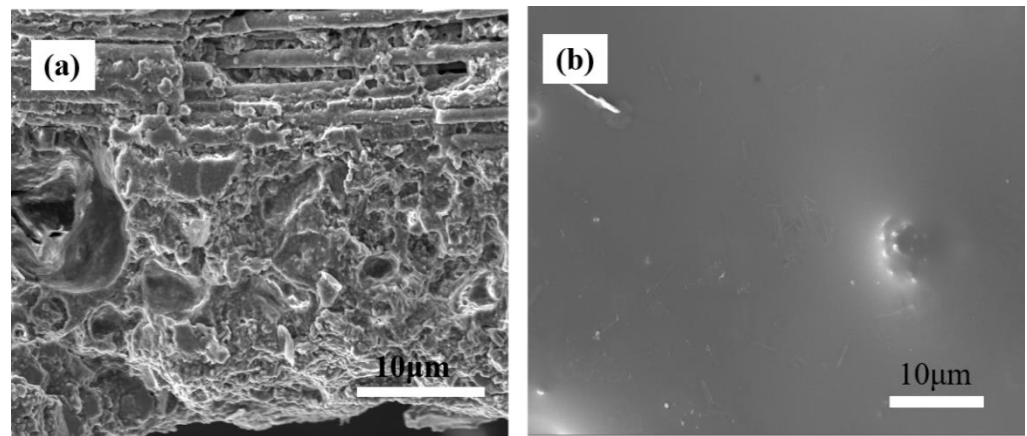


Figure 8. (a) The fracture surface image of coated SiC_f/MWCNTs/AlPO₄ composites after 40 h oxidation and (b) the surface image of the coating after oxidation.

Table 2 shows the results of bend strength, dielectric constants. Obviously, it can be found that the coating is effective in protecting the SiC_f/MWCNTs/AlPO₄ composites from being oxidized.

Table 2. The results of bend strength, dielectric constants.

	Bend Strength/MPa	ϵ'	ϵ''
Pure SiC _f /AlPO ₄ composites		3.6–4.1	0.1–0.2
Coated SiC _f /AlPO ₄ composites		4.2–4.5	0.2–0.5
Coated SiC _f /MWCNTs/AlPO ₄ composites		5.0–6.3	1.8–3.6
Coated SiC _f /MWCNTs/AlPO ₄ composites of oxidation		5.2–6.6	2.3–3.2
Coated SiC _f /MWCNTs/AlPO ₄ composites	205		
Coated SiC _f /MWCNTs/AlPO ₄ composites of oxidation	190		
Uncoated SiC _f /MWCNTs/AlPO ₄ composites of oxidation	60		

Figure 9 shows the schematic diagram of the anti-oxidation mechanism for the coating. During the preparation of the coating, P₂O₅ (g) is readily released while the formation of SiP₂O₇ slows. However, the relatively long oxidation time was enough for P₂O₅ to react with SiO₂ and form SiP₂O₇. Figure 9 gives a summary schematic representation of the mechanism of anti-oxidation based on the results from this study. During the preparation of the coating, the AlPO₄ matrix reacts with SiO₂ to form a SiO₂-AlPO₄ solid solution leading to a strong chemical bond between SiC_f/AlPO₄ composites and the coating. The formation of SiP₂O₇ and SiO₂-AlPO₄ solid solution facilitates the bonding of the particles in the coating, which contributes to the formation of a dense coating. Under oxidizing conditions, the SiC in the coating is partially transformed into SiO₂ as it consumes the incoming oxygen gas, and the decomposition of Al(PO₃)₃ increases with the increasing time. The reactions of SiO₂-AlPO₄ and SiO₂-P₂O₅ occur throughout the coating, linking particles to form a dense coating of low oxygen permeability.

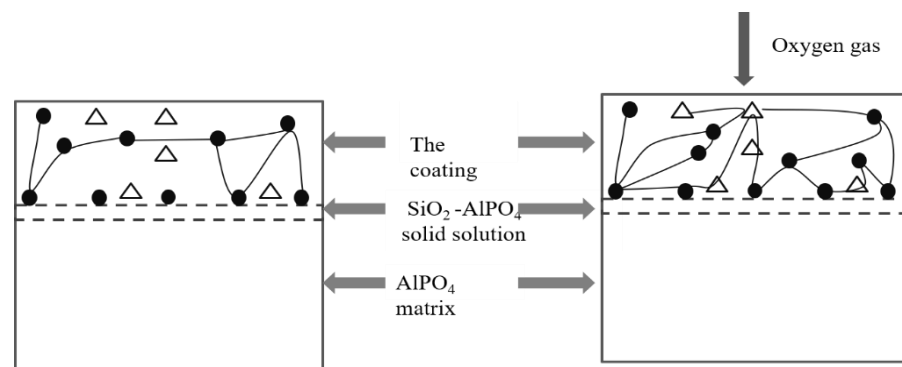


Figure 9. The schematic diagram of anti-oxidation mechanism for the coating (●—AlPO₄, Δ—SiC).

Table 3 shows the calculated Gibbs free energy (ΔG) for the oxidation of SiC at 1273 K. The reaction shown by Code (4) was favored by its minimal value of ΔG . As oxygen gas is introduced, SiC particles are oxidized to SiO₂, which then reacts with P₂O₅ and AlPO₄. The integration of SiO₂, SiP₂O₇, and the SiO₂-AlPO₄ solid solution into the coating is effective in preventing the oxygen gas from further diffusion into the SiC_f/MWCNTs/AlPO₄ composites.

Table 3. The ΔG of SiC oxidation.

Code	Reaction	$\Delta G/\text{kJ/mol}$ at 1273 K
(1)	$\text{SiC} + 1/2\text{O}_2 \rightleftharpoons \text{SiO}(\text{g}) + \text{C}$	−156.07
(2)	$\text{SiC} + \text{O}_2 \rightleftharpoons \text{SiO}_2 + \text{C}$	−632.91
(3)	$\text{SiC} + \text{O}_2 \rightleftharpoons \text{SiO}(\text{g}) + \text{CO}(\text{g})$	−379.94
(4)	$\text{SiC} + 3/2\text{O}_2 \rightleftharpoons \text{SiO}_2 + \text{CO}(\text{g})$	−855.27
(5)	$\text{C} + 1/2\text{O}_2 \rightleftharpoons \text{CO}(\text{g})$	−223.59

4. Conclusions

This study presents a detailed investigation of the anti-oxidation mechanism of the SiO₂ + SiC + Al(H₂PO₄)₃ coating. The anti-oxidation effect of the SiC_f/MWCNTs/AlPO₄ composites in an oxidizing environment (1273 K, 40 h) was confirmed by a three-point bending test, microstructure characterization, and dielectric property. SiC_f/MWCNTs/AlPO₄ composites were chemically bonded with the coating. Oxygen gas in the environment was consumed by SiC particles to form SiO₂, which subsequently reacted with P₂O₅ and AlPO₄ to form SiP₂O₇ and SiO₂-AlPO₄ solid solution, respectively. The integration of SiO₂, SiP₂O₇, and SiO₂-AlPO₄ solid solution into the coating was effective in preventing the oxygen gas from consuming MWCNTs. The coating gives SiC_f/MWCNTs/AlPO₄ composites the potential to be applied as high-temperature structural wave absorbing materials.

Author Contributions: Conceptualization, F.W.; Data curation, J.Y.; Formal analysis, H.X.; Funding acquisition, F.W.; Writing and Investigation—original draft, Y.Z. All authors have read and agreed to the published version of the manuscript.

Funding: This research was funded by the National Natural Science Foundation of China (Grant No. 51802095 and No. 52175167), and the Natural Science Foundation of Hunan Province (Grant No. 2019JJ50165).

Institutional Review Board Statement: Not applicable.

Informed Consent Statement: Not applicable.

Data Availability Statement: Not applicable.

Conflicts of Interest: The authors declare no conflict of interest.

References

1. Hou, Y.; Xiao, B.; Sun, Z.; Yang, W.; Wu, S.; Qi, S.; Wen, G.; Huang, X. High temperature anti-oxidative and tunable wave absorbing SiC/Fe₃Si/CNTs composite ceramic derived from a novel polysilylacetylene. *Ceram. Int.* **2019**, *45*, 16369–16379. [[CrossRef](#)]
2. Kong, L.; Luo, S.; Zhang, G.; Xu, H.; Wang, T.; Huang, J.; Fan, X. Interfacial polarization dominant CNTs/PyC hollow microspheres as a lightweight electromagnetic wave absorbing material. *Carbon* **2022**, *193*, 216–229. [[CrossRef](#)]
3. Lu, J.; Feng, Y.; Liu, J.; Liu, C.; Tong, Y.; Wu, S.; Sun, H.; Gong, H.; Guo, X. Improved electromagnetic wave absorbing performance of PDCs-SiCN(Ni) fibers with different nickel content. *Ceram. Int.* **2022**, *48*, 23578–23589. [[CrossRef](#)]
4. Mo, R.; Ye, F.; Liu, X.; Zhou, Q.; Fan, X.; Xue, J.; Zhang, P.; Zhang, L.; Cheng, L. A high-temperature structural and wave-absorbing SiC fiber reinforced Si₃N₄ matrix composites. *Ceram. Int.* **2021**, *47*, 8191–8199. [[CrossRef](#)]
5. Qin, Z.; Wang, C.; Ma, Y.; Xia, L.; Zhong, B.; Li, X.; Zhang, P. ZIF-67/GNs derived Co₃O₄/GNs multilayer flower and porous structure as an efficient electromagnetic wave absorbing material for excellent absorbing properties. *Appl. Surf. Sci.* **2022**, *575*, 151789. [[CrossRef](#)]
6. Yang, S.; Sun, X.; Wang, S.; Ning, Y.; Yuan, Y.; Yin, W.; Li, Y. Electromagnetic wave absorbing properties of coconut shell-derived nanocomposite. *Carbon* **2022**, *196*, 354–364. [[CrossRef](#)]
7. Ren, Z.; Zhou, W.; Qing, Y.; Xie, H.; Duan, S.; Pan, H.; Lu, X.; Chai, X.; Ran, D.; Zheng, Y. Simultaneous enhancement of mechanical and microwave absorption properties with a novel in-situ synthesis α -Al₂O₃ fillers for SiC_f/SiC composites. *J. Eur. Ceram. Soc.* **2022**, *42*, 4723–4734. [[CrossRef](#)]
8. Zan, Z.; Guo, K.; Sun, J.; Lu, Y.; Yang, B.; Jia, X.; Sivalingam, V.; Xi, J. Investigation on scratching force and material removal mechanism of 3D SiC_f/C-SiC composites during single grain scratching. *J. Eur. Ceram. Soc.* **2022**, *42*, 5366–5379. [[CrossRef](#)]
9. Liégaut, C.; Bertrand, P.; Maillé, L.; Rebillat, F. UHTC-based matrix as protection for C_f/C composites: Original manufacturing, microstructural characterisation and oxidation behaviour at temperature above 2000 °C. *J. Eur. Ceram. Soc.* **2022**, *42*, 3168–3182. [[CrossRef](#)]
10. Jia, J.; Li, C.; Chen, Q.; Bai, S.; Chang, J.; Xiong, D.; Gao, M.; Li, S.; Xiao, J. Effects of SiC content on the mechanical and thermophysical properties of 3D C_f/SiC-Al composites. *Ceram. Int.* **2022**, *48*, 20571–20578. [[CrossRef](#)]
11. Wan, F.; Yan, J.; Xu, H. Enhanced microwave absorbance of oxidized SiC_f/AlPO₄ composites via the formation of a carbon layer on the SiC fibre surface. *J. Eur. Ceram. Soc.* **2018**, *38*, 4356–4362. [[CrossRef](#)]
12. Wan, F.; Luo, F.; Zhou, Y.; Zhou, W.; Zhu, D. A glass coating for SiC fiber reinforced aluminum phosphate matrix (SiC_f/AlPO₄) composites for high-temperature absorbing wave applications. *Surf. Coat. Technol.* **2015**, *264*, 9–16. [[CrossRef](#)]
13. Hu, Y.; Luo, F.; Yang, Z.; Zhou, W.; Zhu, D.; Duan, S. Improvement dielectric and microwave properties of SiC_f/SiC-AlPO₄ composites prepared by precursor infiltration and pyrolysis process. *J. Alloys Compd.* **2017**, *699*, 498–504. [[CrossRef](#)]
14. Wan, F.; Luo, F.; Mu, Y.; Zeng, Z.; Zhou, W. Enhanced mechanical and microwave-absorption properties of SiC_f/AlPO₄ composite with PIP-SiC interphase and the MWCNTs filler. *Ceram. Int.* **2015**, *41*, 9957–9965. [[CrossRef](#)]
15. Zhao, Z.; Li, H.; Zheng, Z.; Zheng, L.; Yan, Y. Improved thermal shock and corrosion resistance of α -Al₂O₃/AlPO₄ coating with PAA addition. *Surf. Coat. Technol.* **2021**, *414*, 127115. [[CrossRef](#)]
16. Wang, T.; Wang, H.; Hong, M.; He, M.; Yang, J.; Ren, K.; Wang, T.; Wang, D. Outstanding enhancements in stability of LiNi_{0.8}Mn_{0.1}Co_{0.1}O₂ cathode by AlPO₄/ACB double coating: Insights into surface structure and chemistry. *Appl. Surf. Sci.* **2022**, *574*, 151663. [[CrossRef](#)]
17. Camarano, A.; Giuranno, D.; Narciso, J. SiC-IrSi₃ for High Oxidation Resistance. *Materials* **2020**, *13*, 98. [[CrossRef](#)]
18. Chen, P.; Xiao, P.; Li, Z.; Liu, Z.; Pu, D.; Li, Y. Microstructure and oxidation behavior of a novel bilayer (c-AlPO₄-SiC_w-mullite)/SiC coating for carbon fiber reinforced CMCs. *J. Eur. Ceram. Soc.* **2019**, *39*, 3988–3999. [[CrossRef](#)]
19. Hao, W.; Huang, J.F.; Cao, L.Y.; Yin, L.X.; Wu, J.P.; Fei, J.; Huang, Y.C.; Yang, L.Q. An AlPO₄-SiC-MoSi₂/SiC oxidation protective coating on carbon/carbon composites by pulse arc discharge deposition. *Ceram. Int.* **2013**, *39*, 9797–9801. [[CrossRef](#)]
20. Sayyed, F.S.; Enayati, M.H.; Nahvi, S.M.; Taghipour, M. Anti-coking and anti-carburizing behavior of amorphous AlPO₄ coating. *Ceram. Int.* **2022**, *48*, 19818–19823. [[CrossRef](#)]
21. Huang, J.F.; Hao, W.; Cao, L.Y.; Yin, L.X.; Ouyang, H.; Yao, C.Y.; Wu, J.P.; Fei, J. An AlPO₄/SiC coating prepared by pulse arc discharge deposition for oxidation protection of carbon/carbon composites. *Corros. Sci.* **2014**, *79*, 192–197. [[CrossRef](#)]
22. Xu, S.; Lu, T.; Shen, K.; Lan, J.; Hu, B.; Zhang, H.; Tang, Y.; Cao, H.; Zheng, G. High temperature oxidation resistance of Ti-5553 alloy with electro-deposited SiO₂ coating. *Mater. Chem. Phys.* **2022**, *275*, 125306. [[CrossRef](#)]
23. Yan, H.J.; Meng, X.Z.; Zhang, Q.H.; Sun, Q.Q.; Wu, L.K.; Cao, F.H. High temperature oxidation performance of the electrodeposited SiO₂ coating incorporated with Ni nanoparticle. *Corros. Sci.* **2022**, *205*, 110455. [[CrossRef](#)]